Journal of Power Sources 195 (2010) 5527–5533

Contents lists available at ScienceDirect

Journal of Power Sources

journal homepage: www.elsevier.com/locate/jpowsour

Structural and electrical properties of Ni–YSZ cermet materials

K. Haberko, M. Jasinski, P. Pasierb, M. Radecka, M. Rekas*

AGH University of Science and Technology, Faculty of Materials Science and Ceramics, 30-059 Cracow, al.Mickiewicza 30, Poland

ARTICLE INFO

Article history:
Received 16 November 2009
Received in revised form 23 February 2010
Accepted 14 March 2010
Available online 20 March 2010

Keywords:
Anode
SOFC
Cermet materials
Ni–YSZ
Electrical properties

ABSTRACT

Ceramic–metal composites (cermets) containing yttria-stabilized zirconia, YSZ, and Ni particles are commonly used as anode materials in solid oxide fuel cells. The long-term performance of fuel cells is strictly related to both the structural and electrical properties of anode materials. In order to achieve high mixed electrical conductivity and high activity of electrochemical reactions and hydrocarbon fuel reforming, it is necessary to select an appropriate chemical composition and a suitable method of preparation. Materials containing 8 mol% yttria-stabilized zirconia and Ni were prepared by means of two methods: co-precipitation and impregnation. The structure of the materials was characterized by means of X-ray diffraction (XRD), scanning electron microscopy (SEM) and porosity studies. The thermal expansion coefficient (TEC) was determined using the dilathometric method. Electrochemical impedance spectroscopy (EIS) and the Wagner polarization method were used to determine electrical conductivity and the electron transference numbers, respectively.

1. Introduction

Nickel-based cermet materials are commonly used as anodes in solid oxide fuel cells [1]. They are used either in two-chamber [1] or single-chamber cells involving oxygen [2], or hydrogen ion conducting solid electrolytes [3]. The properties of such materials are related to the basic functions of the anode, i.e. providing electrochemical reaction sites for the oxidation of fuel, allowing the fuel and by-products to be delivered and removed from the reaction sites, and providing a path for electrons to be transported from the electrolyte/anode interfaces to the interconnects in SOFC stacks. The metallic component acts as the electronic conductor. Moreover, it is an excellent catalyst for breaking hydrogen bonds, shows low reactivity with other cell components, and it can be produced at a fairly low cost. Unfortunately, significant problems arise when using hydrocarbons as cell fuels. For example, the direct oxidation of methane, despite favourable thermodynamics, is a slow process due to carbon deposition. In order to avoid this problem, a gas mixture containing water and methane and with the H_2O/CH_4 ratio greater than three is required [4]. Such a mixture makes it possible to achieve the internal reforming of hydrocarbon on a nickel electrode, while simultaneously preventing the deposition of carbon [5]. High performance anodes require a sufficient concentration of three phase boundaries, TPBs, where fuel molecules and oxygen ions come into contact along electric conduction paths. Such concentration can be obtained using materials exhibiting sufficiently open porosity. More than 30% (by volume) of open porosity is required to facilitate the transport of fuel and product gases. However, using only the nickel phase as an anode material, there are still 2D metal/electrolyte contacts where the TPBs are located, due to the fact that oxygen ions originate from the electrolyte only. Moreover, there are several other problems. For example, the thermal expansion coefficient (TEC) of nickel is considerably higher than that of some electrolytes, such as YSZ, which may result in the deterioration of the cell. Furthermore, nickel easily sinters at higher temperatures, which results in a decrease in the porosity of the anode. All these problems are solved by using a composite anode involving a matrix of YSZ and nickel particles. The YSZ phase provides a component of ionic conductivity, and nickel particles form the electron path through the anode. Such a solution leads to a substantial enlargement of the electrochemical reaction zone, and enhances the electrode stability and adherence to the electrolyte, and, most importantly, adjusts the thermal expansion coefficients [6,7]. Moreover, the YSZ forms a frame for the dispersion of metallic particles and provides the necessary mechanical durability in the case of the anode supported cells. Since the anode material should provide percolation paths for electrons, oxygen ions and gases, the electrochemical performance is closely related to the electrode microstructure [8–10].

The Ni–YSZ cermet anode is commonly fabricated by directly mixing NiO and YSZ powders, which are subsequently reduced by the fuel in SOFCs [1]. The reduction of NiO to Ni results in the desirable porosity of the anode. However, some authors proposed adding pore-forming additions like graphite, starch, etc., in order to establish suitable porosity (40–60%) for the gas flow. Using such a method of cermet anode preparation, consisting in mixing YSZ

* Corresponding author. Tel.: +48 126174722; fax: +48 126341201.
E-mail address: rekas@agh.edu.pl (M. Rekas).

0378-7753/$ – see front matter © 2010 Elsevier B.V. All rights reserved.
doi:10.1016/j.jpowsour.2010.03.050

with NiO powder, sufficient electronic and ionic conductivity may be achieved when the concentration of Ni in the composite is above 30 vol.% [1] (above 40 wt.%).

Taking into account the fact that the performance of the anode is strongly influenced by its microstructure, which is determined by the method of preparation, we decided to study Ni–YSZ cermets prepared by two other methods: co-precipitation and impregnation.

The aim of this work was to determine the effect of the cermet preparation method on both the structural and the electrical properties of the cermet. Two preparation methods were used: co-precipitation and impregnation.

2. Experimental

2.1. Preparation of materials

2.1.1. Co-precipitation

Aqueous solutions of zirconium nitrate with an appropriate amount of yttrium nitrate and nickel nitrate – as a precursor of nickel – were introduced into an ammonia solution. The resulting gels were washed with water, dried, and calcined at the temperature of 700 °C for 1 h. The powders were ground in a mortar, pressed into pellets under 200 kPa, and then sintered in air at 1300 °C for 3 h. The weight% of nickel in the obtained material amounted to 50%.

2.1.2. Impregnation

Pellets from pure yttria-zirconia were prepared in a similar way to that described above, i.e. by means of co-precipitation of zirconium and yttrium nitrates in the same ammonia solution. The main difference was that only after co-precipitation were they impregnated with nickel nitrate and calcined until the weight% of nickel reached 30 and 48.

In the case of both procedures, the pellets were reduced for 6 h in 5% H_2/Ar at 800 °C. Such conditions are sufficient to completely reduce of the NiO reduction to Ni [11–14].

2.2. Microstructure and XRD analysis

The phase composition of all sintered samples was characterized by means of X-ray diffraction analysis. Measurements were performed on a Philips X'Pert MPD diffractometer within the range of diffraction angles 2θ from 10° to 80°, and with Cu–K filtered radiation. Crystallographic and phase analysis was carried out by means of an implemented program of line profile analysis, LPA. Open porosity was measured using the water saturation method. Scanning electron microscopy (SEM) equipped with Energy-Dispersive X-ray Analyzing System (EDX) observations of powders were recorded with a FEI NOVA NanoSEM 200 equipped with a BSED detector.

2.3. Dilathometric studies

Dilathometric studies were carried out in a prototypical dilathometer, with the measuring instrument and "size changing" transducer provided by Jota. Cuboidal samples of the dimensions: $2 \times 2 \times 9$ mm were used for the experiments. The measurements were carried out in an argon atmosphere at the temperature range of 20–800 °C. The coefficients of thermal expansion were calculated for all samples.

2.4. Electrochemical impedance spectroscopy

The purpose of the impedance spectroscopy measurement was to determine an equivalent circuit and resulting charge transfer mechanism of studied materials. The electrical properties of yttria-zirconia-based solutions were investigated by ac-electrochemical impedance spectroscopy in the temperature range of 20–800 °C and at frequencies (f) from 1 Hz to 400 kHz. The measurements were taken on a Solartron SI1260 Impedance/Gain-Phase Analyzer with the SI 1287 Electrochemical interface. Prior to the electrical measurements, the Pt electrodes ($\phi = 5$ mm) were screen-printed (Demerton Pt paste) from both sides of the cylindrical samples ($\phi = 7$ mm, $d = 2$ mm) and fired at 800 °C for 5 min in an Ar + 5% H_2 gas atmosphere. Fig. 1a illustrates the design of the measured samples measured with Pt electrodes.

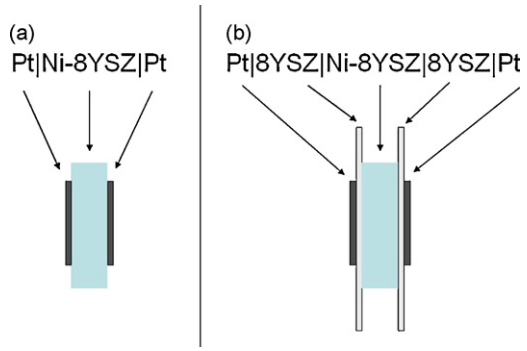

Fig. 1. Experimental setup used to determine I–U characteristics, (a) without electron-blocking electrodes; (b) with electron-blocking YSZ layers.

Table 1
Chemical composition, porosity and TEC of the Ni–ZrO_2^+ 8 mol% Y_2O_3 specimens, prepared using either the impregnation or the co-precipitation method.

Sample	wt.% Ni	Method of preparation	Porosity [%]	TEC [10^6 K^{-1}]
30N	30	Impregnation	49.2[a]	11.3
48N	48	Impregnation	49.2[a]	13.2
50N	50	Co-precipitation	50.8	15.1

[a] Porosity of YSZ (before of impregnation).

2.5. Current–voltage characteristics

Partial conductivities of YSZ-Ni composite materials were determined using the symmetrical Wagner method [14]. Two types of

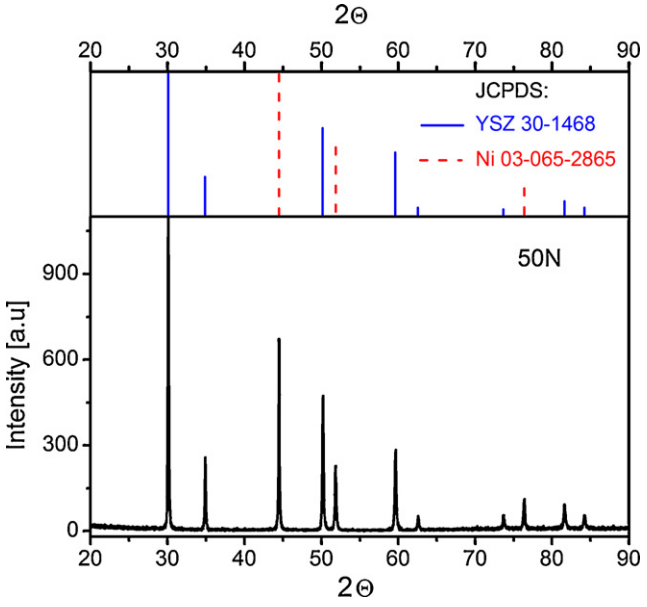

Fig. 2. XRD pattern of the 50N sample.

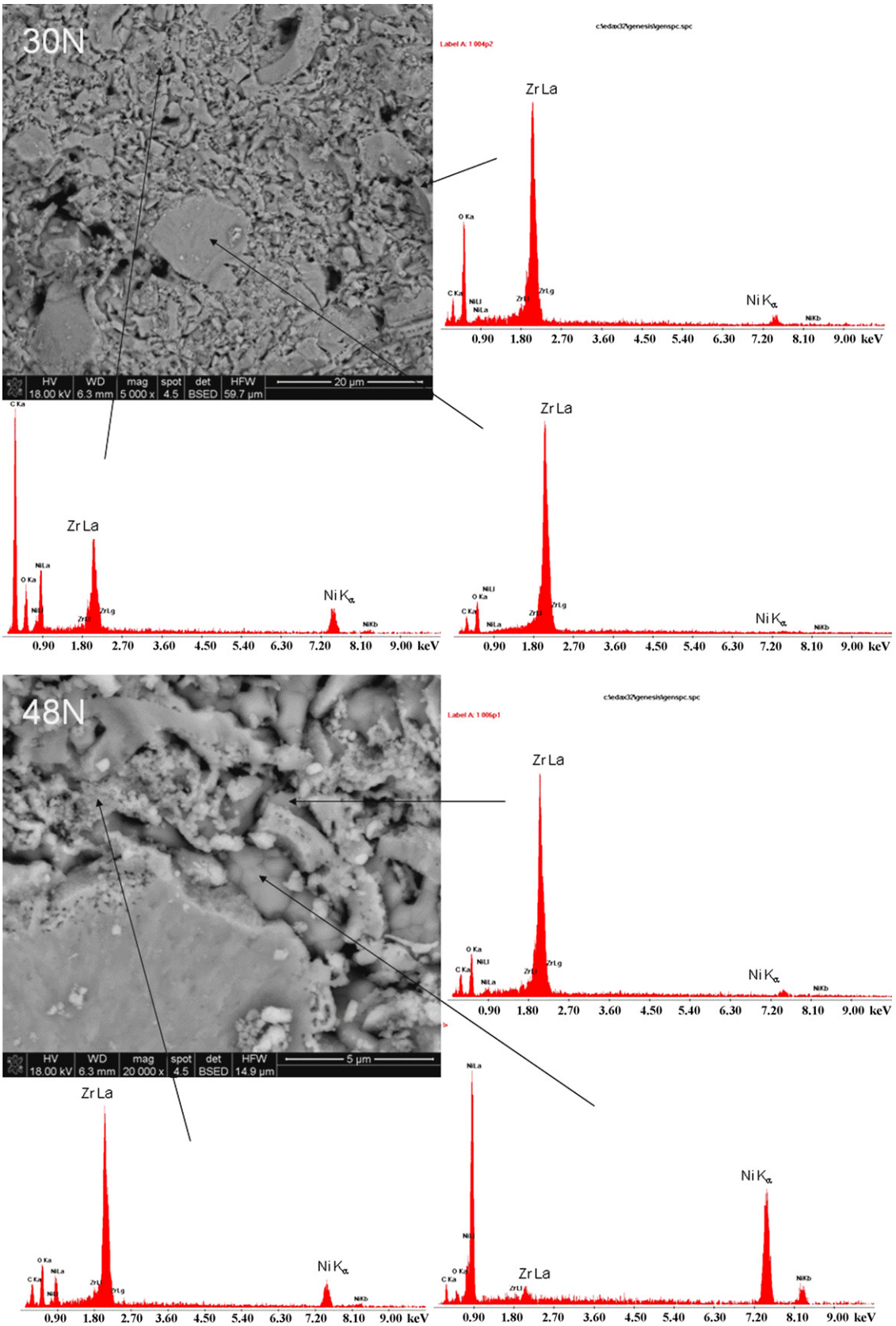

Fig. 3. SEM micrographs and EDX spectra of the studied materials. 0N, 48N and 50 N denote the studied samples containing 30, 48 and 50 wt.% Ni, respectively.

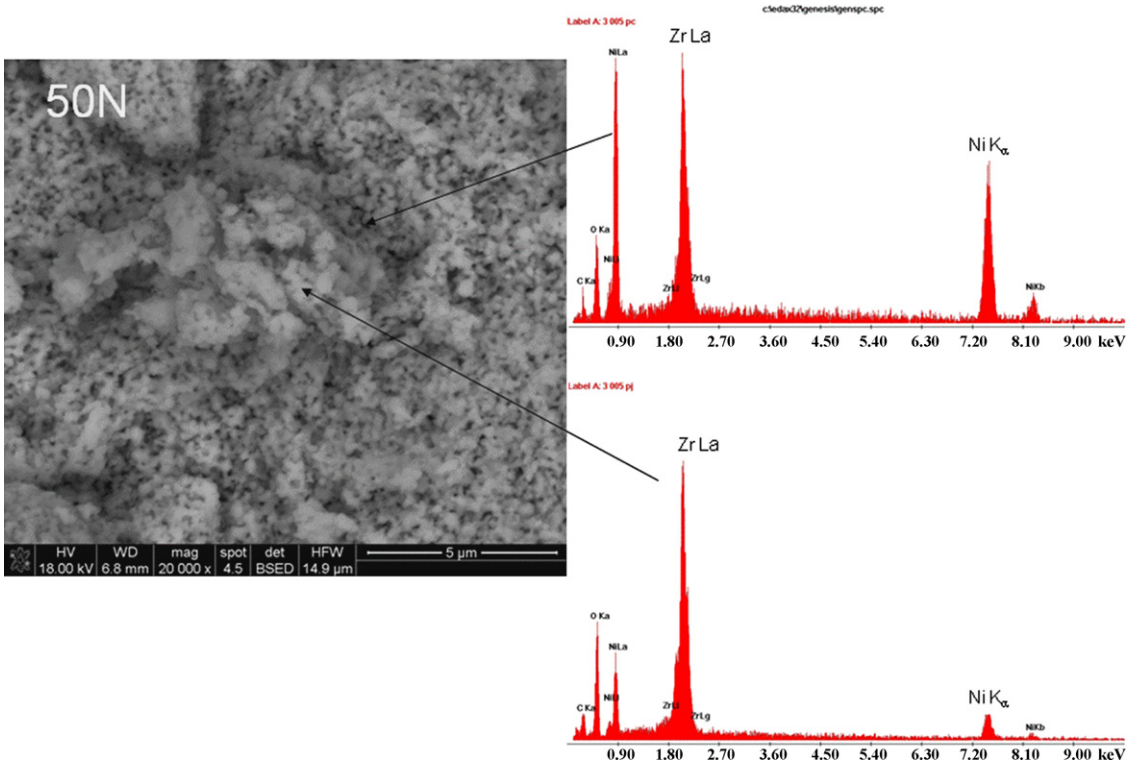

Fig. 3. (*Continued*).

electrodes were used, as shown in Fig. 1. In the case of porous Pt electrodes (left figure), the total conductivity was measured, while for Pt|YSZ electrodes (right figure) only the ionic conductivity of oxygen ions was determined due to the electron-blocking properties of YSZ. 8YSZ dense plates, with a thickness of 100 μm, were used as the electron-blocking electrodes. The ionic electrical resistance of the plates was at least 10% lower than that of the studied Ni–8YSZ sample. The electronic conductivity was calculated from:

$$\sigma_{el} = \sigma_{total} - \sigma_{ion} \quad (1)$$

where σ_{total}, σ_{el} and σ_{ion} denote the total, electronic and ionic conductivities, respectively. The conductivities were calculated from the results of *I–U* measurements, taking into account the geometry of the samples (diameter $\varphi = 7$ mm, thickness $d = 2$ mm).

The measurements were carried out in the temperature range 25–750 °C in gas flow (60 $cm^3\ min^{-1}$) in the reducing atmosphere (Ar + 5 vol.% H_2). A Keithley 2420 SMU controlled by the TestPoint program was used as a voltage source (from −2 to 2 V) and current meter.

3. Results and discussion

The basic data for the obtained samples, including the chemical composition, method of preparation, porosity and TEC are shown in Table 1. All samples exhibit a porosity of ca. 50%, which is suitable for fuel cell anode performance [15,16]. It should be emphasized that such porosity was obtained without the addition of any pore-forming agents (like graphite, organic components, etc.). It was observed that the thermal expansion coefficient of Ni–YSZ cermet increases linearly with nickel content [17]. The determined TEC's are between the values of YSZ ($10.5 \times 10^{-6}\ K^{-1}$) [1] and Ni ($17.0 \times 10^{-6}\ K^{-1}$) [18]. However, according to the values presented in Table 1, the TEC of impregnated samples is ca. 11% lower than that of the co-precipitated samples, as calculated for the same Ni concentration (50 wt.%). This is beneficial as far as the match between the TECs of the two adjacent phases – the anode and the electrolyte – is concerned, and makes it possible to avoid the cracking of the cell during operation.

Fig. 2 shows the XRD pattern of the studied sample marked as 50N (according to Table 1). The diffraction pattern is typical for highly crystalline materials. It was found that the samples are composed from Ni and YSZ phases. No additional phases were found. In particular, the lack of NiO reflexes indicates complete reduction of the cermet.

Similar results were obtained for other materials. In particularly, lack of the NiO reflexes confirms that reduction of NiO powder to Ni was complete.

SEM micrographs and EDX spectra of the sintered samples are shown in Fig. 3. All samples are composed of nano-grains of nickel, which forms a continuous phase. A tendency of YSZ nano-grains to agglomerate into larger ones (several μm in diameter) is observed in the case of the 30N and 48N materials. On the other hand, nanometric grains of YSZ are visible for 50N, i.e. the sample prepared through co-precipitation (Fig. 3), which is much more uniform than the samples prepared through impregnation (30N and 48N). In the samples containing between 30 and 50 wt.% Ni, the percolation threshold was exceeded.

The experimental Nyquist plots on the complex impedance plane at 673 K are presented in Fig. 4. The complex component Z'' (reactance) assumes constant values for frequencies lower than 100 kHz. This may suggest that the equivalent circuit of the studied samples consists of *R–L* connected in series (*R* – resistor, *L* – inductor). The parameters of *L* and *R* obtained by fitting the experimental data (within the frequency range 0.1 Hz to 100 kHz) to the equivalent circuit consisting of *R–L* connected in series (*R* – resistor, *L* – inductor) are listed in Table 2. The values of *L* vary between 2.6 and 2.7 μH, and the values of *R* are around 2 Ω. These parameters are typical for Ni paths in the studied cermet materials. Point symbols in Fig. 5 illustrate the experimental results on the complex admittance plane. Both solid and dashed lines represent the theoretical dependencies of the *R–L* circuit plotted for the *R* and *L* parameters from Table 2. As can be seen, the agreement between

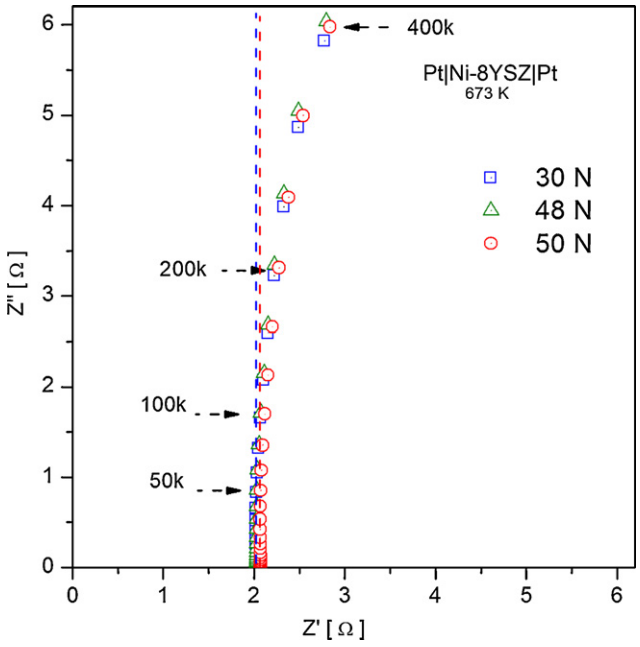

Fig. 4. Experimental Nyquist plots of the studied samples at 673 K on the complex impedance plane. Numbers denote frequencies, *f*, in kHz; e.g. 400k corresponds to *f* = 400 kHz.

Table 2
Inductance, *L*, and resistance, *R* and resistivity ρ; ρ_{EIS} from the EIS measurements, and ρ_{dc} from the dc experiments of the studied materials, at 673 K.

Sample	*L* (H)	*R* (Ω)	ρ_{EIS} (Ω cm)	ρ_{dc} (Ω cm)
30N	$(2.634 \pm 0.005) \times 10^{-6}$	2.026 ± 0.001	1.985 ± 0.001	5.18 ± 0.33
48N	$(2.66 \pm 0.01) \times 10^{-6}$	2.033 ± 0.002	1.992 ± 0.002	4.64 ± 0.31
50N	$(2.59 \pm 0.01) \times 10^{-6}$	2.072 ± 0.002	2.031 ± 0.002	4.75 ± 0.16

the experimental and the theoretical values is quite satisfactory for frequencies lower than 100 kHz. However, noticeable discrepancy between the two sets of data is observed above 100 kHz.

The inductance component in the equivalent circuit was usually omitted by other authors. Dees et al. [19] observed no frequency dependence of impedance on the complex impedance plane for the Ni/YSZ cermet at 1000 °C. A similar plot for our results is illustrated in Fig. 5. The differences observed between Dees et al. [17] and our

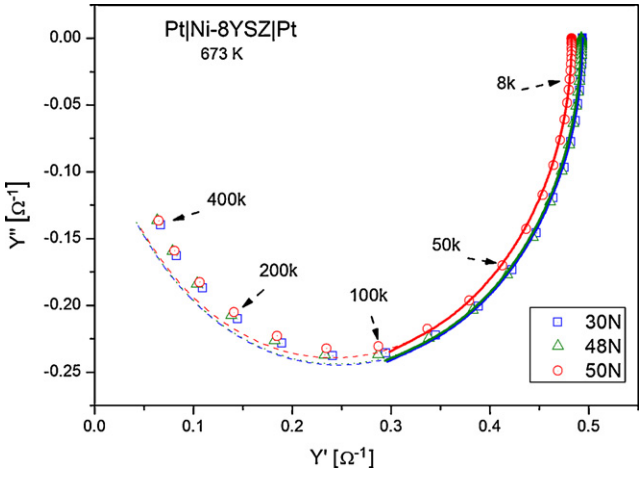

Fig. 5. Experimental Nyquist plots of the studied samples at 673 K on the complex admittance plane. Points—experimental results; lines—theoretical dependencies. Numbers denote frequencies, *f*, in kHz; e.g. 400k corresponds to *f* = 400 kHz.

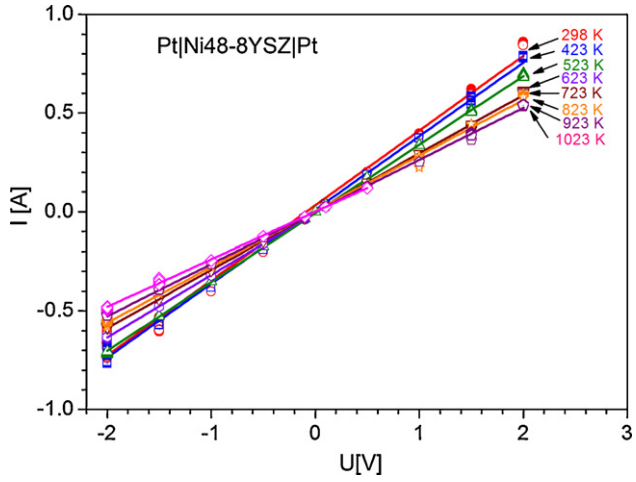

Fig. 6. Current (*I*) versus voltage (*U*) of the Pt|Ni48–8YSZ|Pt system at several temperatures.

results may be explained by different frequency ranges in the two works.

Fig. 6 shows the current–voltage characteristics of the Pt|Ni48–8YSZ|Pt specimen at several temperatures. Similar dependencies were observed for other samples. The straight line dependencies show that the studied materials exhibit ohmic behavior.

The slopes of the straight lines in Fig. 6 correspond to the total electrical conductivity. As can be seen, the total electrical conductivity decreases with temperature. Dees et al. [19] fitted this dependence using Arrhenius-like equation with negative activation energy equal to $-(0.0591 \pm 0.001)$ eV.

Fig. 7 illustrates temperature dependence of the total electrical resistivity in the coordination system: ρ_{total} versus temperature, *T*. Electrical resistivity increases with temperature, for all studied samples. The observed increase of resistivity, $\rho(T)$, with temperature indicates that the metallic conductivity component predominates over the ionic one. The metallic conductivity of the studied materials, may be attributed to the presence of nickel particles in cermet materials. Generally, the increase of resistivity with temperature is typical for metallic phases. However, the shape of the $\rho(T)$ dependence may differ substantially depending on the mechanism of charge scattering [20]. Apart of temperature dependence ρ_{total}, electrical resistivity of the cermet materials changes with the porosity. This dependence is usually expressed by Brugge-

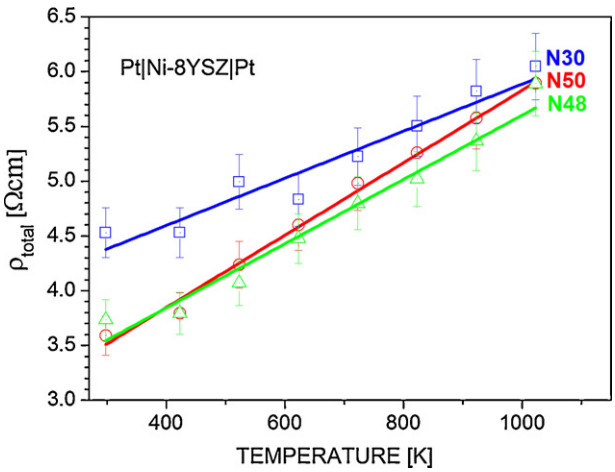

Fig. 7. Temperature dependence of total resistivity (ρ_{total}).

Table 3
Temperature dependencies of total (ρ_{total}) and ionic (ρ_{ion}) conductivities and literature data activation energy of ionic conductivity of YSZ.

Sample	$\rho_{total} = A + BT$		$\sigma_{ion} = \frac{\sigma_0}{T} \exp\left(-\frac{E_{act}}{kT}\right)$	
	A [Ω cm]	B [Ω cm K^{-1}]	E_{act} [eV]	$\log \sigma_0/[\Omega^{-1}\,cm^{-1}\,K]$
30N	3.74 ± 0.16	(2.15 ± 0.24) × 10^{-3}	0.93 ± 0.02	3.77 ± 0.16
48N	2.67 ± 0.14	(2.93 ± 0.23) × 10^{-3}	0.85 ± 0.03	3.48 ± 0.22
50N	2.52 ± 0.08	(3.31 ± 0.12) × 10^{-3}	0.88 ± 0.10	3.73 ± 0.72

Sample	E_{act} [eV]	Ref.
8YSZ	0.8	Baumard and Abelard [22]
	1.05	Pimenov et al. [23]
	0.76	Gong et al. [24]
	1.11–1.14	Martin and Mecartney [25]
	0.89 ± 0.02	Wierzbicka et al. [26]

man equation [21]:

$$\rho_{total} = \rho_b \left(1 - \frac{p}{100}\right)^{-3/2} \quad (2)$$

where ρ_{total} is the effective resistivity of the cermet, ρ_b is the bulk resistivity (anporous material) and p is porosity in % of the cermet. Inserting $p = 50\%$ into Eq. (2) we have: $\rho_{total} \approx 2.8\rho_b$. The current–voltage characteristics of the studied materials registered at the electron-blocking electrodes, i.e. Pt|8YSZ|Ni–8YSZ|8YSZ|Pt, differ substantially from those recorded at the porous Pt electrodes. Fig. 8 shows the typical results in the case of 48N. For the same voltages, the registered current is about 3 orders of magnitude lower for the electron-blocking electrodes than for the Pt electrodes. Furthermore, when the temperature is altered, the slopes exhibit opposite tendencies depending on which type of electrode is used. Fig. 9 presents the temperature dependencies of the ionic electrical conductivity, σ, in the coordinate system: $\log(\sigma T)$ versus T^{-1}. Determined total resistivity from the dc experiments corresponding to 673 K were listed in column ρ_{dc} of Table 2. The values ρ_{dc} (from dc experiments) are ca. 2.3–2.5 times higher than that ρ_{EIS} (from impedance measurements). This discrepancy can result from the polarization phenomena accompanying to dc experiments.

Table 3 illustrates the activation energy, E_{act}, determined from the temperature dependence of the ionic conductivity. E_a varies between 0.85 and 0.92 eV, and is typical for the 8YSZ solid electrolyte [22–26].

Based on presented electrical property studies we can conclude that the preparation methods described in this work leads to obtain sufficiently high electronic conductivity for the concentration of Ni in the cermet that is much lower (30 wt.%) than that used the traditional preparation method (above 30 vol.% = 40 wt.%) [1,19]. This means that the preparation method and the resulting microstructure have much higher impact on the electrical properties of the Ni–YSZ cermet materials than chemical composition.

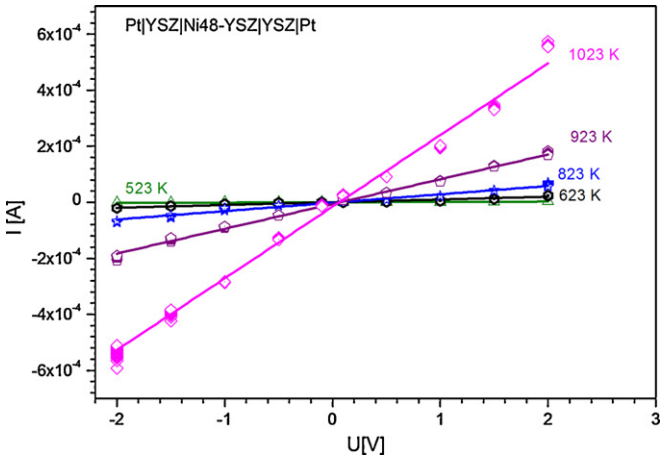

Fig. 8. Current (I) versus voltage (U) of the Pt|8YSZ|Ni48–8YSZ|8YSZ| Pt system at several temperatures.

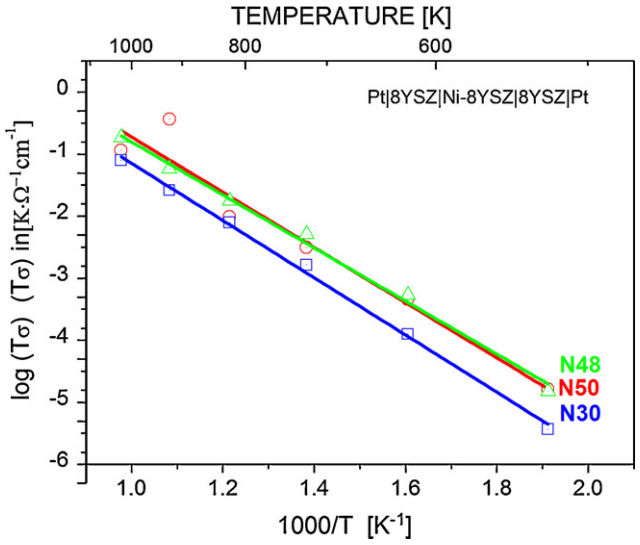

Fig. 9. Arrhenius plots of $\log(T\sigma)$ of ionic conductivity.

Using both the total electrical resistivity, ρ (Fig. 7), and ionic conductivity, σ (Fig. 8), we can determine the electron transference numbers from the relationship:

$$t_{el} = \frac{\sigma_{el}}{\sigma_{total}} = \frac{(1/\rho_{total}) - \sigma_{ion}}{(1/\rho_{total})} \quad (3)$$

Determined electron transference numbers revealed that the overall charge transport within temperature range 298–1023 K is predominantly electronic in nature ($1 > t_{el} \geq 0.99$).

4. Conclusions

Cermet materials containing ZrO_2 + 8 mol% Y_2O_3 (8YSZ) and Ni particles were prepared using two methods: co-precipitation and impregnation. Both proposed preparation methods provide suitable anode materials for SOFCs. XRD analysis revealed that the materials were composed from well crystallized phases of 8YSZ and Ni. Their porosity was ca. 50%. The proposed preparation methods make it possible to obtain sufficient open porosity without adding any pore-forming additions.

The thermal expansion coefficients (TECs) varied between 11×10^{-6} and 15×10^{-6} K^{-1}. Lower values of the TECs (closer to those of the 8YSZ electrolyte) are observed for the samples prepared by means of the impregnation method.

Electrochemical impedance spectroscopy was used to determine the electrical properties of the studied materials. The equivalent circuit used for fitting the impedance spectra consists of *R*–*L* elements connected in series. It was found that the *R*–*L* model circuit represents the experimental circuit within 0.1 Hz to 100 kHz well. The temperature dependence of electrical resistivity remains in qualitative agreement with metallic properties. Determined electron transference numbers revealed that the overall charge transport is predominantly electronic in nature.

Acknowledgements

The financial support of The Polish Ministry of Science and Higher Education (grant no. R15 019 02) is gratefully acknowledged.

References

[1] N.Q. Minh, T. Takahashi, Science and Technology of Ceramic Fuel Cells, Elsevier, Amsterdam, 1995.
[2] M. Yano, A. Tomita, M. Sano, T. Hibino, Solid State Ionics 177 (2007) 3351.
[3] L.N. Van Rij, J. Le, Van Landschoot, J. Schoonman, J. Mater. Sci. 36 (2001) 1069.
[4] S. Park, R. Craciun, J.M. Vohs, J. Gorte, J. Electrochem. Soc. 146 (1999) 3603.
[5] T. Iida, M. Kawano, T. Matsui, R. Kikuchi, K. Eguchi, J. Electrochem. Soc. 154 (2007) B234.
[6] D. Sarantaridis, A. Atkinson, Fuel cells 7 (2007) 246.
[7] E.V. Tsepis, V.V. Kharton, J. Solid State Electrochem. 12 (2008) 1039.
[8] W.Z. Zhu, S.C. Deevi, Mater. Sci. Eng. A 362 (2003) 228.
[9] B. Nait-Ali, K. Haberko, H. Vesteghem, J. Absi, D.S. Smith, J. Eur. Ceram. Soc. 26 (2006) 3567.
[10] H. Abe, W.-J. Moon, M. Naito, Fuel Cells Bull. (2006) 12.
[11] Y.-Y. Chen, W.-Ch. J. Wei, Solid State Ionics 177 (2006) 351.
[12] B. Liu, Y. Zhang, B. Tu, Y. Dong, M. Cheng, J. Power Sources 165 (2007) 114.
[13] M. Lang, C. Auer, A. Eismann, P. Szabo, N. Wagner, Electrochim. Acta 53 (2008) 7509.
[14] R.W. West, N.M. Tallan, J. Appl. Phys. 36 (1965) 543.
[15] J.-H. Lee, J.-W. Heo, D.-S. Lee, J. Kim, G.-H. Kim, H.-W. Lee, H.S. Song, J.-H. Moon, Solid State Ionics 158 (2003) 225.
[16] H. Abe, K. Murata, W.-J. Moon, K. Kaneko, M. Nito, Fuel Cell Bull. (2006) 12.
[17] N.Q. Minh, J. Am. Ceram. Soc. 76 (1993) 563.
[18] S.-D. Kim, H. Moon, S.-H. Hyun, J. Moon, J. Kim, H.-W. Lee, Solid State Ionics 178 (2007) 1304.
[19] D.W. Dees, T.D. Claar, T.E. Easler, D.C. Fee, F.C. Mrazek, J. Electrochem. Soc. 134 (1987) 2141.
[20] P.R.N. Childs, Practical Temperature Measurement, Butterworth-Heinemann, 2001, p. 172.
[21] D.A.G. Bruggeman, Ann. Phys. 24 (1935) 636.
[22] J.F. Baumard, P. Abelard, in: N. Claussen, M. Rühle, A.H. Heuer (Eds.), Science and Technology of Zirconia II, Advances in Ceramics, vol. 12, American Ceramic Society, Columbus, 1984, pp. 557–571.
[23] A. Pimenov, J. Ulrich, P. Lukenheimer, A. Loidl, C.H. Rüscher, Solid State Ionics 109 (1998) 111.
[24] J. Gong, Y. Li, Z. Zhang, Z. Tang, J. Am. Ceram. Soc. 83 (2000) 648.
[25] M.C. Martin, M.L. Mecartney, Solid State Ionics 171 (2003) 67.
[26] M. Wierzbicka, P. Pasierb, M. Rekas, Phys. B 387 (2007) 302.